A Real-Time Articulated Human Motion Tracking Using Tri-Axis Inertial/Magnetic Sensors Package

Rong Zhu and Zhaoying Zhou

***Abstract*—A basic requirement in virtual environments is the tracking of objects, especially humans. A real time motion-tracking system was presented and evaluated in this paper. System sensors were built using tri-axis microelectromechanical accelerometers, rate gyros, and magnetometers. A Kalman-based fusion algorithm was applied to obtain dynamic orientations and further positions of segments of the subject's body. The system with the proposed algorithm was evaluated via dynamically measuring Euler orientation and comparing with other two conventional methods. An arm motion experiment was demonstrated using the developed system and algorithm. The results validated the effectiveness of the proposed method.**

***Index Terms*—Fusion algorithm, human motion tracking, inertial/magnetic sensors.**

I. Introduction

REAL-TIME human motion tracking has many applications in such fields ranging from virtual reality to medicine. There are currently several fundamental tracking technologies, such as mechanical tracking, electromagnetic tracking, acoustic tracking, optical tracking, and inertial/magnetic tracking. Among these, inertial/magnetic tracking technology has currently attracted many interests as such method is free of most of the problems of other technologies. An inertial/magnetic tracking system uses a combination of accelerometers, rate gyros, and magnetic sensors [2]. There is no inherent latency associated with inertial/magnetic sensing, all delays are due to data transmission and processing [1]. Another benefit with inertial/magnetic sensing is its sociability, i.e. sourceless, whereas electromagnetic, acoustic, and optic devices all require emissions from a source to track objects. Since micromachined sensors have become generally available, human motion can be tracked continuously outside of a laboratory with quite smaller, lighter, and ambulatory measurement system.

Previously, a three-dimensional (3-D) accelerometer unit was used as an inclinometer on the assumption that the magnitude of the acceleration can be neglected with respect to the gravity [3], [4]. This method, however, gave unacceptable errors in dynamic human motion recording. Another popular applied method was to estimate orientation by integrating angular rate measured with rate gyros [5], [6]. Nevertheless, an error in measured angular rate would result in an increasing inaccuracy in the estimated orientation. Integrating multisensor signals of rate gyros and accelerometers to estimate orientation was, thus, introduced for dealing with these above problems [7]. The fusion technology for integrating multisensor signals to estimate orientation was commonly based on a nonlinear Kalman filter by using a nonlinear quaternion model [8] so that the computation was quite complicated.

Manuscript received August 14, 2003; revised December 26, 2003.

The authors are with the Department of Precision Instruments and Mechanology, Tsinghua University, Beijing 100084, China (e-mail: zr-wzwyj@sh163.net).

Digital Object Identifier 10.1109/TNSRE.2004.827825

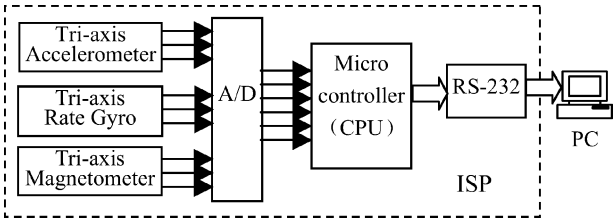

Fig. 1. Block diagram of ISP.

Research is currently being conducted at Tsinghua University for tracking human motion with the use of microelectromechanical accelerometers, rate gyros, and magnetometers. An integrated sensor pack (ISP) was developed to estimate the object's orientation. An improved linear Kalman filter was designed to process the sensor signals to estimate desired sensing variables of gravity and magnetic field, and further yield orientation and position of the object. In the tracking system, axis-angle pairs consisting of a joint angle and a rotation axis rather than the conventional Euler angles were applied to represent orientations of human segments. Unlike the Euler expression, the axis-angle pairs avoid Euler angles' singularities associated with gimbal rotation axes, and have computational efficiency and compactness with only a single rotation rather than three successive Euler rotations.

II. Hardware Design

Each ISP acting together as a unit consisted of a tri-axis microelectromechanical accelerometer, tri-axis micro rate gyro, tri-axis micro magnetometer, A/D converter, a micro controller, and RS-232. Fig. 1 indicates the composing of an ISP. An experimental prototype of ISP, which was quite small and light with approx 40 g each, was developed. The prototype was comprised of two ADXL202 accelerometers (two-axis accelerometer with ± 2 g measurement range, about 200 $\mu g\sqrt{Hz}$ noise density), a pair of Honeywell's HMC1001/1002 magnetometers (single-axis/two-axis magnetic sensors with ± 2-G measurement range, about 4-μG noise level), and three Murata's ENV-05F-03 rate gyroscopes (single-axis gyroscope with $\pm 60°/s$ measurement range and about 0.004 °/s noise level) so as to form a tri-axis multisensor configuration. Additional circuitry periodically sampled all tri-axis sensors

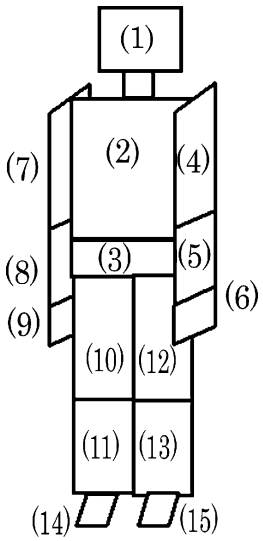

Fig. 2. Depiction of the 15 segments comprising stick figure for human body.

and transmitted the data through an RS-232 to a personal computer for post-processing. Software in the computer then processed the received sensor readings and determined the spatial orientation of the object that the ISP was attached to.

III. Algorithm Design

To realize motion tracking for a human body, it is necessary to make a model corresponding more closely to the human skeleton in overall proportion and relative placement and attachment. In addition, the model should remain mathematically simple. Conventionally, the human body was represented as stick figure [9], a human virtual rendering standards model articulated structure using segments and joints. The body segments could be approximated as consecutive lines. Therefore, a 15-segment humanoid was developed using Hanavan's model [10], see Fig. 2. Unlike the orientation expression used in convention, which described the orientation of the segment by three successive Euler rotations about specified axes to bring the Earth coordinate into alignment with the body coordinate, a geometric representation was used to calculate segment motion parameters. Specifically the orientation of each segment was described as a rotation about a single inclined axis. The parameters of the segments, such as joint angles and rotation axes, addressed human body motion.

A. Orientation Representation

In order to better understand the relationship between tri-axis sensors' readings on a segment and the respective orientation representation of the segment, a model depicted in Fig. 3 was employed. In this model, segment i having a tri-axis ISP at its midsection was represented by an orthogonal frame with three orthogonal axes X_i, Y_i, and Z_i. The sensitive axes of the tri-axis sensors were X_i, Y_i, and Z_i, also. And the other orthogonal frame with three axes X_{i+1}, Y_{i+1}, and Z_{i+1} represented its conjoint segment $i+1$, which had another ISP at its midsection with X_{i+1}, Y_{i+1}, and Z_{i+1} as the sensor axis.

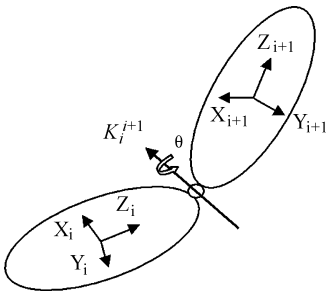

Fig. 3. Physical segment model and the definition of its orthogonal frame.

The tri-axis ISP produces readings that correspond to the respective dot product of an effect vector along each sensor axis. Specifically a tri-axis accelerometer on the segment i produces three components of the acceleration of the segment along X_i, Y_i, and Z_i, a tri-axis magnetometer on the segment i produces three components of magnetic field along X_i, Y_i, and Z_i, and a tri-axis gyro on the segment i produces three components of the angular rate of the segment along X_i, Y_i, and Z_i. To embody the orientation between the two connective segments, we defined an angle θ as the joint angle by which the segment $i+1$ was rotated with respect to the segment i, and an axis K_i^{i+1} as the rotation axis about which the segment $i+1$ was rotated. Based on the orientation representation of the joint angle and the rotation axis, the rotation matrix $\mathrm{Rot}(K_i^{i+1}, \theta)$ between the coordinate frames of the segment i and the segment $i+1$ can be represented as (1), see the equation at the bottom of the page, where $K_i^{i+1} = [K_x, K_y, K_z]$ denotes the standard orthonormal basis of the rotation axis K_i^{i+1} in frame $X_i - Y_i - Z_i$, $\mathrm{Vers}\theta = 1 - \cos\theta$.

The output of tri-axis accelerometer $\vec{a}$ is normally expressed as follows:

$$\vec{a} = \vec{g} + \vec{a}_l + \vec{\varepsilon} \tag{2}$$

where $\vec{g}$, $\vec{a}_l$, and $\vec{\varepsilon}$ denote the gravity acceleration, the linear acceleration, and noise in sensor coordinate frame. Since the gravity acceleration $\vec{g}$ can be considered as a uniform vector for any object, it is desired to pick $\vec{g}$ out from the output of accelerometer and combine it with the magnetometer to estimate orientation of the object.

Assume that the linear acceleration $\vec{a}_l$ has been subtracted from the accelerometer output and the noise $\vec{\varepsilon}$ is neglected. By the rotation matrix $\mathrm{Rot}(K_i^{i+1}, \theta)$, the relationship between the

$$\mathrm{Rot}\left(K_i^{i+1}, \theta\right) = \begin{bmatrix} K_x^2 Vers\theta + \cos\theta & K_x K_y Vers\theta - K_z \sin\theta & K_x K_z Vers\theta + K_y \sin\theta \\ K_x K_y Vers\theta + K_z \sin\theta & K_y^2 Vers\theta + \cos\theta & K_y K_z Vers\theta - K_x \sin\theta \\ K_x K_z Vers\theta - K_y \sin\theta & K_y K_z Vers\theta + K_x \sin\theta & K_z^2 Vers\theta + \cos\theta \end{bmatrix} \tag{1}$$

corresponding sensor measurements of the two ISPs respectively attached to the segment i and the segment $i+1$ is expressed as

$$\left[g_x^{i+1}\ g_y^{i+1}\ g_z^{i+1}\right]^T = \mathrm{Rot}\left(K_i^{i+1},\theta\right)\cdot\left[g_x^i\ g_y^i\ g_z^i\right]^T \quad (3)$$

$$\left[H_x^{i+1}\ H_y^{i+1}\ H_z^{i+1}\right]^T = \mathrm{Rot}\left(K_i^{i+1},\theta\right)\cdot\left[H_x^i\ H_y^i\ H_z^i\right]^T \quad (4)$$

where $[g_x^i\ g_y^i\ g_z^i]^T$ and $[g_x^{i+1}\ g_y^{i+1}\ g_z^{i+1}]^T$ denote the gravity components in $X_i - Y_i - Z_i$ and $X_{i+1} - Y_{i+1} - Z_{i+1}$ measured by the two sets of tri-axis accelerometer attached to the segment i and the segment $i+1$, respectively. $[H_x^i\ H_y^i\ H_z^i]^T$, $[H_x^{i+1}\ H_y^{i+1}\ H_z^{i+1}]^T$ are the magnetic components of the earth's magnetic field measured by the two sets of tri-axis magnetometer attached to the segment i and the segment $i+1$, respectively. In practice, the accurate measurement of the uniform earth's magnetic field by magnetometers is affected by nearby ferrous materials in the environment. The measurement distortions from the environment influence can be categorized as hard iron and soft iron effects. The hard iron distortions arise from permanent magnets and magnetized substances in a fixed location relative to the magnetic sensors. These distortions will remain constant and can be compensated by calibration methods associated with specified rotations of the magnetic sensor in order to sample the magnetic space surrounding the sensor [11], [12]. The soft iron distortions arise from the interaction of the earth's magnetic field and any magnetically soft material in the environment. Compensating for soft iron effects is more difficult than for hard iron effects since the effects vary from location to location. In our study, we suggested to take the magnetic sensors as far as possible from magnetic materials in the environment so as to avoid the soft iron effects to the most extent.

Equations (3) and (4) are used to figure out the joint angle θ and the rotation axis K_i^{i+1}, which is specified as axis-angle pairs to represent the orientation of the segment $i+1$ with respect to the segment i. The joint angle θ is a positive value representing the magnitude of the rotation, and the direction attribute of the rotation is embodied by the rotation axis K_i^{i+1}. The rotation matrix $\mathrm{Rot}(K_i^{i+1},\theta)$ can also be equivalently expressed by conventional Euler angles (commonly specified as pitch α, roll γ and heading ψ)

$$\mathrm{Rot}\left(K_i^{i+1},\theta\right) = \begin{bmatrix} \cos\psi\cos\alpha & \sin\psi\cos\alpha & -\sin\alpha \\ \cos\psi\sin\alpha\sin\gamma & \sin\psi\sin\alpha\sin\gamma & \cos\alpha\sin\gamma \\ -\sin\psi\cos\gamma & +\cos\psi\cos\gamma & \\ \cos\psi\sin\alpha\cos\gamma & \sin\psi\sin\cos\gamma & \cos\alpha\cos\gamma \\ +\sin\psi\sin\gamma & -\cos\psi\sin\gamma & \end{bmatrix}. \quad (5)$$

In solving (3)–(5), the Euler angles can be determined from the gravity and magnetic measurements as well. To estimate human motion, the axis-angle pairs take advantages than the Euler expression in virtue of nonsingularity and simple computation with only a single rotation θ rather than three successive Euler rotations α, γ, and ψ. In addition, the joint angle allows the implementation of joint limits, which match the motion limits of a human skeleton.

B. Dynamic Design Using Kalman Algorithm

In the (5), an assumption has been made that the linear acceleration is quite small to be neglected, or it can be subtracted from the accelerometer output. For most dynamic situations, the kinematic linear acceleration normally is in existence, which, therefore, must be eliminated from the accelerometer output. Thus, we combined a tri-axis accelerometer and a tri-axis magnetometer with a tri-axis rate gyro to estimate the desired sensing components.

When considering the dynamic process, we set two time points t and $t+\Delta t$ (that $\Delta t \to 0$) as a start point and an end point of a process, and developed the rotation matrix for the segment i. In this rotation process, the time gap Δt was set to be very short that the rotation angle (i.e., $\Delta\theta$) of the segment i was small to yield $\cos\Delta\theta \approx 1$, and $\sin\Delta\theta \approx \Delta\theta$. Thus, the rotation matrix could be simplified as

$$\mathrm{Rot}\left(K_i^i(\Delta t),\Delta\theta\right) = \begin{bmatrix} 1 & -K_z^i(t)\cdot\Delta\theta & K_y^i(t)\cdot\Delta\theta \\ K_z^i(t)\cdot\Delta\theta & 1 & -K_x^i(t)\cdot\Delta\theta \\ -K_y^i(t)\cdot\Delta\theta & K_x^i(t)\cdot\Delta\theta & 1 \end{bmatrix} \quad (6)$$

where $K_i^i(\Delta t) = \lfloor K_x^i(t), K_y^i(t), K_z^i(t)\rfloor$ denotes the rotation axis of the segment i in the segment frame $X_i - Y_i - Z_i$. Then, the dynamic rotation of the segment i from the time t to the time $t+\Delta t$ could be expressed by means of the following multiplications:

$$\left[g_x^i(t+\Delta t)\ g_y^i(t+\Delta t)\ g_z^i(t+\Delta t)\right]^T = \mathrm{Rot}\left(K_i^i(\Delta t),\Delta\theta\right)\cdot\left[g_x^i(t)\ g_y^i(t)\ g_z^i(t)\right]^T \quad (7)$$

$$\left[H_x^i(t+\Delta t)\ H_y^i(t+\Delta t)\ H_z^i(t+\Delta t)\right]^T = \mathrm{Rot}\left(K_i^i(\Delta t),\Delta\theta\right)\cdot\left[H_x^i(t)\ H_y^i(t)\ H_z^i(t)\right]^T \quad (8)$$

where $[g_x^i(t)\ g_y^i(t)\ g_z^i(t)]^T$ and $[g_x^i(t+\Delta t)\ g_y^i(t+\Delta t)\ g_z^i(t+\Delta t)]^T$ are the acceleration components in the segment i frame at times t and $t+\Delta t$, respectively, and $[H_x^i(t)\ H_y^i(t)\ H_z^i(t)]^T$ and $[H_x^i(t+\Delta t)\ H_y^i(t+\Delta t)\ H_z^i(t+\Delta t)]^T$ are the magnetic components in the segment i frame at times t and $t+\Delta t$, respectively.

Rearrange (7) and (8), and consider $\Delta t \to 0$ to yield an equivalent equation as follows:

$$\begin{bmatrix} \dot g_x^i \\ \dot g_y^i \\ \dot g_z^i \\ \dot H_x^i \\ \dot H_y^i \\ \dot H_z^i \end{bmatrix} = \begin{bmatrix} 0 & -\omega_z^i & \omega_y^i & 0 & 0 & 0 \\ \omega_z^i & 0 & -\omega_x^i & 0 & 0 & 0 \\ -\omega_y^i & \omega_x^i & 0 & 0 & 0 & 0 \\ 0 & 0 & 0 & 0 & -\omega_z^i & -\omega_z^i \\ 0 & 0 & 0 & \omega_z^i & 0 & -\omega_x^i \\ 0 & 0 & 0 & -\omega_y^i & \omega_x^i & 0 \end{bmatrix} \cdot \begin{bmatrix} g_x^i \\ g_y^i \\ g_z^i \\ H_x^i \\ H_y^i \\ H_z^i \end{bmatrix} \quad (9)$$

where $\omega_x^i = K_x^i(t)\cdot(\Delta\theta/\Delta t)|_{\Delta t\to 0}$, $\omega_y^i = K_y^i(t)\cdot(\Delta\theta/\Delta t)|_{\Delta t\to 0}$, and $\omega_z^i = K_z^i(t)\cdot(\Delta\theta/\Delta t)|_{\Delta t\to 0}$ denote the components of the angular velocity along axes X_i, Y_i, and Z_i, respectively, which can be measured by the tri-axis rate gyro of the ISP attached to the segment i.

A Kalman filter was then applied to make estimations of desired gravity and magnetic components. Regard

$\vec{S}^i = [g_x^i\ g_y^i\ g_z^i\ H_x^i\ H_y^i\ H_z^i]^T$ as state variables, and use (9) to be state model of Kalman filter. Since the measurement data to the filter are provided by sensors, it is natural to choose the sensor vectors (i.e., the measurements of accelerometer and magnetometer) as the output $\vec{Z}^i$ of the Kalman filter, so that yields a linear identity measurement equation

$$\vec{Z}^i = \vec{S}^i + \vec{\delta}^i \tag{10}$$

where $\vec{\delta}^i$ is measurement noise.

Based on Kalman iterated algorithm [13] using (9) and (10), the state variables $\vec{S}^i$ were estimated. Since the estimated variables $\vec{S}^i$ are derived from the hybrid of accelerometer, gyro, and magnetometer, it incorporates excellent dynamics of gyro and stable drift-free performance of gravity acceleration and magnetic field. We estimated the variables $\vec{S}^i$ and $\vec{S}^{i+1}$ for the segment i and the segment $i+1$, and then estimated the orientation of the segment i with respect to the segment $i+1$ via solving (3) and (4).

C. Using Tri-Axis Inertial/Magnetic Sensors Package to Measurement Human Motion

Based on Hanavan's model, a measurement system incorporating 15 ISPs over nonjoint locations of a wearer's body must be developed. Then, determine 15 orientations for the 15 segments by the sensor readings of the attached ISPs. Integrating orientations and physical dimensions of the segments can further figure out the position of the target segment with respect to an initial segment by using rotation and displacement transfer starting from the initial segment. We developed a local transfer matrix $\mathrm{Trans}_i^{i+1}(\theta_i, l_i)$ consisting of the segment's rotation and displacement information as follows:

$$\mathrm{Trans}_i^{i+1}(\theta_i, l_i) = \begin{bmatrix} \mathrm{Rot}\left(K_i^{i+1}, \theta_i\right) & \begin{matrix}0\\0\\l_i\end{matrix} \\ 0\,0\,0 & 1 \end{bmatrix} \tag{11}$$

where θ_i, l_i denote the joint angle and the physical length of the segment i. To estimate position of the segment i with respect to the initial coordinate frame of the initial segment, sequential multiplication of the local transfer matrixes of the consecutive segments to obtain a global transfer matrix A_1^i from the initial segment to the segment i was performed. Generally, select the feet standing on the ground as the initial segment

$$\begin{aligned} A_1^i &= \begin{bmatrix} n_x & o_x & a_x & p_x \\ n_y & o_y & a_y & p_y \\ n_z & o_z & a_z & p_z \\ 0 & 0 & 0 & 1 \end{bmatrix} \\ &= \mathrm{Trans}_1^2(\theta_1, l_1) \cdots \mathrm{Trans}_{i-1}^i(\theta_{i-1}, l_{i-1}) \\ &\quad \cdot \mathrm{Trans}_i^i(0, l_i) \end{aligned} \tag{12}$$

where $\begin{bmatrix} n_x & o_x & a_x \\ n_y & o_y & a_y \\ n_z & o_z & a_z \end{bmatrix}$ denotes the rotation matrix from the initial coordinate frame to the coordinate frame of the segment i and $[p_x\ p_y\ p_z]^T$ denotes the position vector of the segment i in the coordinate frame of the initial segment.

IV. Experimental Method

A. Measurement of Orientation Using Kalman Algorithm

For evaluating the performance of the proposed Kalman algorithm, we performed an experiment to measure Euler orientation (i.e., pitch, roll, and heading) using a developed ISP prototype. The experiment was performed like the hardware prototype was manually manipulated to move back and forth on a horizontal plane, therefore, with up-and-down linear acceleration along the horizontal directions. The pitch and the roll would remain constant during the horizontal motion (i.e., zero). The heading angle suffered from a bit fluctuation around a constant value due to the manipulation error. The proposed Kalman algorithm was used to estimate orientation with 20-Hz updating rate. For comparison, an integral algorithm with tri-axis rate gyro [14] and a direct gravity and magnetic solution [15] with tri-axis accelerometer and magnetometer were also tested, respectively.

In addition, the dynamic rotation measurement of the prototype was further tested on a single-axis rotating table. Took the pitch angle as an example. Fixed the prototype on the working platform of the rotating table, and put the pitch axis of the prototype along the rotation axis of the table. We drove the rotating table to rotate back and forth about the axis of rotation. The reference angles and the measured angles derived from the proposed Kalman algorithm were compared.

B. Measurement of Human Motion

For testing the multijoint movement and validating the effectiveness of the proposed method using for tracking human motion, a real arm motion was performed. Three ISPs were attached to the subject's upper trunk, right upper arm, and right lower arm, respectively. The subject faced to an upright wall, on which the fourth ISP was attached. The Z axis of the fourth ISP pointed in the vertical direction, upwards. The X axis of the fourth ISP was normal to the wall, inward, and the Y axis was horizontal. The subject moved the upper trunk and let the three axes X, Y, and Z of the ISP attached on the upper trunk along to the three axes X, Y, and Z of the ISP on the wall. The physical lengths of the upper arm and the lower arm were measured to be approximately 31.5 and 30.5 cm, respectively. The physical dimension of the upper trunk was approximately 13 cm in width (distance from the center of the ISP on the upper trunk to the right shoulder joint in the Y direction) and 19 cm in height (distance from the center of the ISP on the upper trunk to the right shoulder joint in the Z direction). Make the upper trunk unmoveable so as to fix the upper trunk frame X–Y–Z, then shook the right arm to let the end of the lower arm move along a horizontal line (i.e., parallel with Y axis) and a vertical line (i.e., parallel with Z axis) on the wall, respectively. The separate desired sensing variables for the upper trunk, the upper arm and the lower arm were estimated by the proposed linear Kalman filter. Then, the estimated variables were imported to (3) and (4) to figure out the orientations of the corresponding segments. The rotation matrixes derived from the orientations and the physical dimensions of the upper trunk, the upper arm and the lower arm were used in (12) to calculate the instantaneous position of the

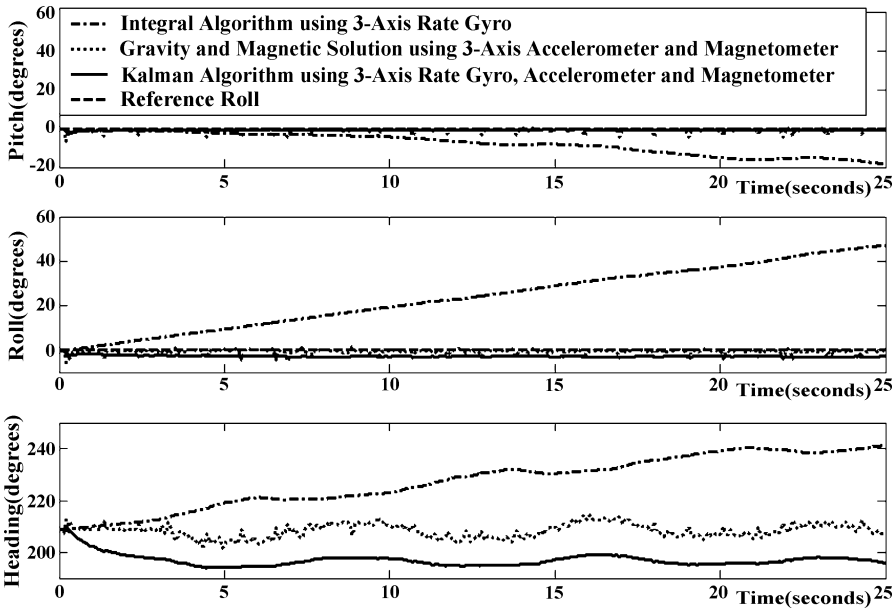

Fig. 4. Orientation estimation by three algorithms.

end of lower arm with respect to the upper trunk's coordinate frame. Specifically, the calculation was formulated as

$$A_1^3 = \begin{bmatrix} n_x & o_x & a_x & p_x \\ n_y & o_y & a_y & p_y \\ n_z & o_z & a_z & p_z \\ 0 & 0 & 0 & 1 \end{bmatrix} = \begin{bmatrix} & & & 0 \\ \multicolumn{3}{c}{\mathrm{Rot}\left(K_1^2, \theta_1\right)} & -13 \\ & & & 19 \\ 0 & 0 & 0 & 1 \end{bmatrix} \cdot \begin{bmatrix} & & & 0 \\ \multicolumn{3}{c}{\mathrm{Rot}\left(K_2^3, \theta_2\right)} & 0 \\ & & & 31.5 \\ 0 & 0 & 0 & 1 \end{bmatrix} \cdot \begin{bmatrix} 1 & 0 & 0 & 0 \\ 0 & 1 & 0 & 0 \\ 0 & 0 & 1 & 30.5 \\ 0 & 0 & 0 & 1 \end{bmatrix} \tag{13}$$

where $\mathrm{Rot}(K_1^2, \theta_1)$ denotes the rotation matrix from the upper trunk to the upper arm, θ_1 is the joint angle. $\mathrm{Rot}(K_2^3, \theta_2)$ denotes the rotation matrix from the upper arm to the lower arm, θ_2 is the joint angle. $[p_x\ p_y\ p_z]^T$ denotes the instantaneous position vector of the end of the lower arm in the coordinate frame of the upper trunk.

V. Experimental Result

A. Measurement of Orientation Using Kalman Algorithm

Fig. 4 depicted the comparative results of the measurements of Euler orientations using three algorithms. Note that the reference values of the pitch and the roll (dashed line) during the motion were zero. It could be seen that the solution only using three-axis accelerometer and magnetometer (dotted line) was affected by the moving acceleration and obvious errors occurred in the estimations of the angles. The orientation obtained by the integral algorithm (dashdotted line) had increasing drift as time increases. In contrast, the result under the proposed linear Kalman algorithm (solid line) displayed better performance, i.e., the standard deviations from the reference values (i.e., zero) were approximately 0.2° for pitch and roll. The standard deviation of heading angle was about 1.5°. The fluctuation of the heading angle was mostly due to the manipulation error.

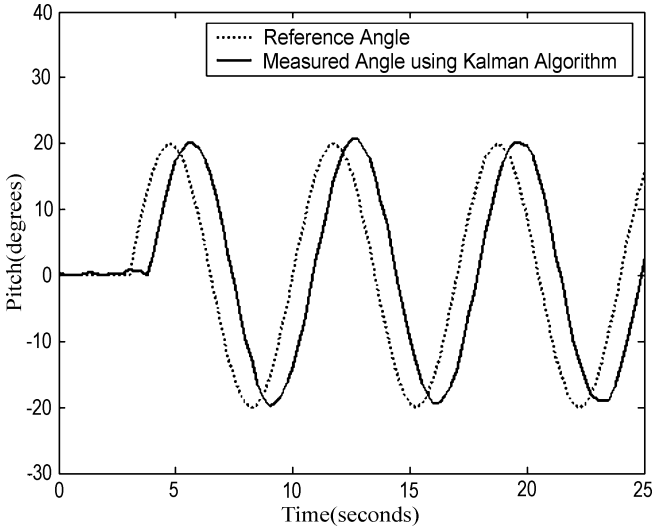

Fig. 5. Comparison of the reference rotation with the measurement of the proposed Kalman algorithm.

Aiming at the dynamic rotation measurement for the prototype, a comparison between the reference angles and the measured angles using the proposed Kalman algorithm was shown in Fig. 5. The dynamic error of the pitch measurement was about 1°. Obviously there existed a time lag between the reference angle and the measured angle due to Kalman filter. The time lag of our prototype was about 0.9 s.

B. Measurement of Human Motion

For the arm motion, Fig. 6 and Fig. 7 illustrate the calculated position of the end of the lower arm with respect to the upper trunk and the joint angles between the two consecutive segments in the two movements. In the horizontal movement,

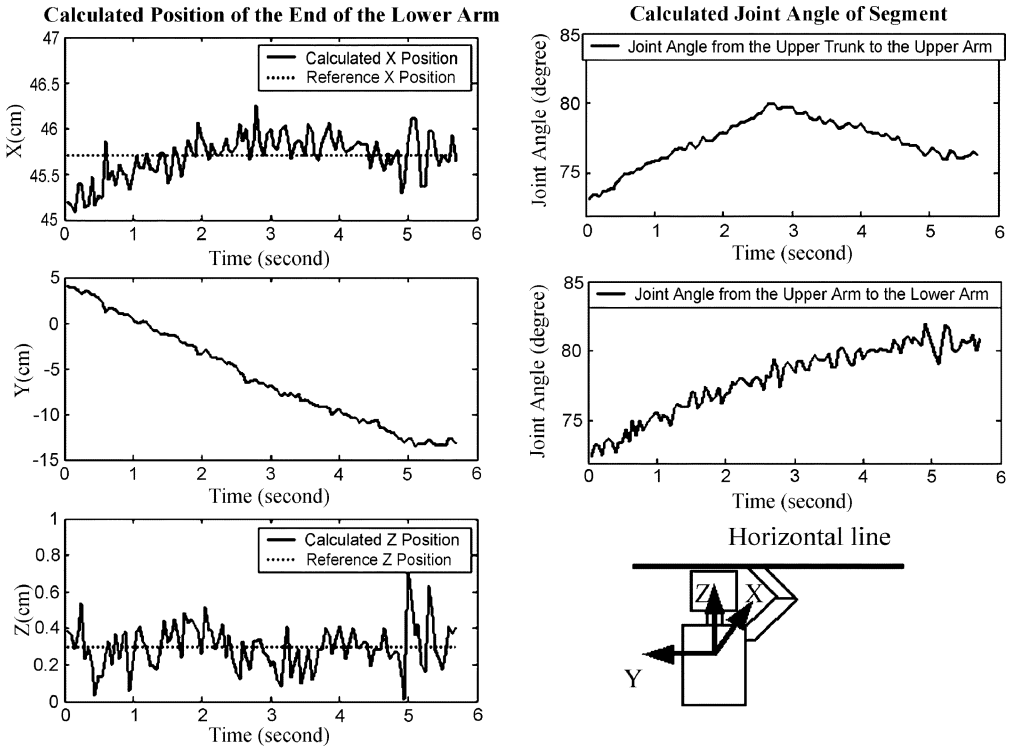

Fig. 6. Calculated position and joint angle in horizontal movement.

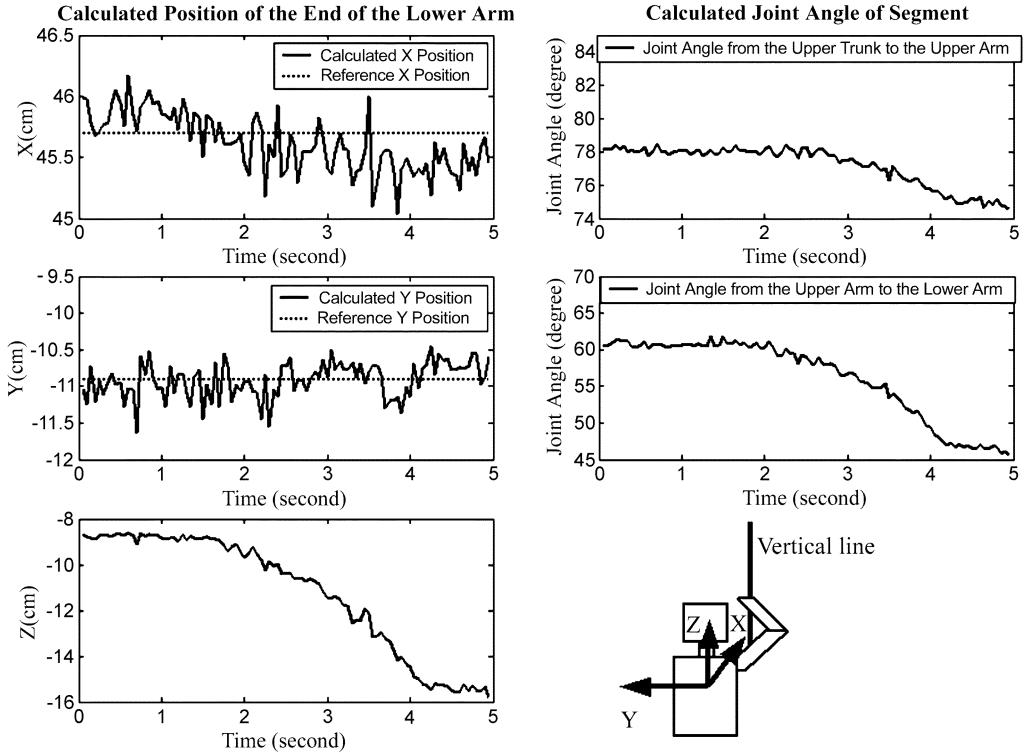

Fig. 7. Calculated position and joint angle in vertical movement.

the reference position of the end of the lower arm in the X and Z directions remained constant and was shown as dotted lines, see Fig. 6. In the vertical movement, the reference X and Y positions of the end of the lower arm remained constant as well and was shown as dotted lines, see Fig. 7. Both Fig. 6 and 7 showed that the errors of the calculated positions were less than 1 cm. Since the position of the end segment was calculated by integrating the orientations and the positions of the fore corresponding segments, the accurate measurement of the end segment position was largely affected by the measurement errors from all corresponding ISPs' sensors and the approximation of the physical dimensions of the corresponding segments.

VI. Discussion

In this paper, we presented a measure to deal with the problem of tracking human motion by using micro inertial/magnetic sensors with a Kalman-based algorithm. Our investigation revealed that the conventional measurement using integral angular rate measured by rate gyros to get orientations would arouse increasing drift errors, and the previous method based on incline-principle using accelerometers would suffer by the disturbance of linear accelerations. The experimental comparisons among the different methods showed that utilizing the Kalman filter to integrate accelerometers with rate gyros and magnetometers could incorporate excellent dynamics of gyro and stable drift-free performance of gravity acceleration and magnetic field. The proposed linear Kalman model, where the sensing components of gravity and magnetic field are as state variables, can benefit to make the algorithm realized more easily.

Our study also revealed that the proposed Kalman algorithm would, unfortunately, cause a time lag existing in the measurement (shown in Fig. 5) when using the ISPs and the proposed Kalman algorithm to get orientations in the real application. For damping this lag, we can consider to add a variance of the driving noise (i.e., the random part of the dynamic state model) in the state model of the filter so that the Kalman filter in effect has a fading memory built into it [13]. The filter fading rate can be controlled adaptively to prevent lag error buildup. However, there exists a conflict between the time lag and the random estimation error, i.e., the shorter the lag, but the larger the random error of the filter. This results in a compromise being needed [13].

Aiming at the human motion tracking, we believed utilizing the derived orientations and physical dimensions of the segments to figure out the position of the target segment by sequential multiplication of local transfer matrixes of the consecutive segments was a feasible and facilitated method. The experimental results of an arm motion tracking (shown in Fig. 6 and Fig. 7) indicated that the tracking could also be very accurate, e.g., the error of the position measurement for the end of the lower arm could be less than 1 cm. The accuracy of the derived position of the target segment was largely dependent on the measurement accuracy of the orientations and physical dimensions of all corresponding segments.

Our next step of the work will include increasing the number of ISP units and extending the multijoint measurement to all segments of the body for tracking the whole body motion.

VII. Conclusion

This paper presented a method to track orientations and positions of human segments for a rendition of 3-D human motion. The method utilized tri-axial microelectromechanical sensors, such as accelerometers, rate gyros and magnetometers, to figure out the defined axis-angle pairs of each segment based on the proposed linear Kalman algorithm. Integrating orientations and physical dimensions of the segments could further figure out the segments' spatial positions by sequential rotation and displacement transfers starting from an initial segment. The real human motion tracking was demonstrated via an experiment of an arm motion.

Acknowledgment

The authors would like to thank T. Yu and D. Wang for help on the experiments.

References

[1] G. Wu and Z. Ladin, "The study of kinematic transients in locomotion using the integrated kinematic sensor," *IEEE Trans. Rehab. Eng.*, vol. 4, pp. 193–200, Sept. 1996.

[2] E. Bachmann, I. Duman, U. Usta, R. McGhee, X. Yun, and M. Zyda, "Orientation tracking for humans and robots using inertial sensors," in *Proc. Int. Symp. Computational Intelligence in Robotics and Automation (CIRA)*, 1999, pp. 187–194.

[3] B. Kemp, A. J. M. W. Janssen, and B. van der Kamp, "Body position can be monitored in 3D using miniature accelerometers and earth-magnetic field sensors," *Electroencephalogr. Clin. Neurophysiol./Electromyogr. Motor Contr.*, vol. 109, no. 6, pp. 484–488, 1998.

[4] P. H. Veltink, "Detection of static and dynamic activities using uniaxial accelerometers," *IEEE Trans. Rehab. Eng.*, vol. 4, pp. 375–385, Dec. 1996.

[5] J. E. Bortz, "A new mathematical formulation for strapdown inertial navigation," *IEEE Trans. Aerosp. Electron. Syst.*, vol. 7, pp. 61–66, 1971.

[6] M. B. Ignagni, "Optimal strapdown attitude integration algorithms," *J. Guidance*, vol. 12, no. 2, pp. 363–369, 1990.

[7] G. Baselli, "Assessment of inertial and gravitational inputs to the vestibular system," *J. Biomech.*, vol. 34, no. 6, pp. 821–826, 2001.

[8] J. L. Marins, X. P. Yun, and E. R. Bachmann, "An extended Kalman filter for quaternion-based orientation estimation using MARG sensors," in *Proc. 2001 IEEE/RSJ Int. Conf. Intelligent Robots and Systems*, 2001, pp. 2003–2011.

[9] L. W. Campbell and A. F. Bobick, "Recognition of human body motion using phase space constraints," in *Proc. 5th Int. Conf. Computer Vision*, 1995, pp. 624–630.

[10] P. Corbeil, M. Simoneau, D. Rancourt, A. Tremblay, and N. Teasdale, "Increased risk for falling associated with obesity: Mathematical modeling of postural control," *IEEE Trans. Neural Syst. Rehab. Eng.*, vol. 9, pp. 126–136, June 2001.

[11] B. Hoff and R. Azuma, "Autocalibration of an electronic compass in an outdoor augmented reality system," in *Proc. IEEE ACM Int. Symp. Augmented Reality*, Oct. 2000, pp. 159–164.

[12] M. J. Caruso, "Applications of magnetic sensors for low cost compass systems," in *Proc. Position Location and Navigation Symp., IEEE 2000*, Mar. 2000, pp. 177–184.

[13] E. Brookner, *Tracking and Kalman Filtering Made Easy*. New York: Wiley-Interscience, 1998, ch. 18, pp. 375–382.

[14] P. G. Savage, "Strapdown inertial navigation integration algorithm design," *J. Guid., Contr., Dynam.*, pt. 2: Velocity and Position Algorithms , vol. 21, no. 2, pp. 208–221, 1998.

[15] R. Zhu, "A novel miniature azimuth-level detector based on MEMS," in *Proc. Microelectromechanical Systems Conf.*, vol. 24, 2001, pp. 50–53.

Rong Zhu was born in 1968. She received the B.S., M.S., and Ph.D. degrees in instrument engineering from Shanghai Jiao Tong University, Shanghai, China, in 1990, 1993, and 1999, respectively.

From 1993 to 2000, she was with the Instrument Engineering Department, Shanghai Jiao Tong University, where she had been an Associate Professor since 1999. Since 2002, she has been an Associate Professor with Department of Precision Instruments, Tsinghua University, Beijing, China. Her research interests include automation, navigation and guidance, and microelectromechanical systems.

Zhaoying Zhou was born in 1937. He received the B.S. degree from the Department of Precision Instruments, Tsinghua University, Beijing, China, in 1961.

From 1979 to 1981, he was a Visiting Scientist with the Department of Automatic Control, Lund University, Lund, Sweden. Since 1987, he has been a Professor and Head of the MEMS Laboratory of the Department of Precision Instruments, Tsinghua University. He is also an Editor of the *International Journal of Micromechatronics*. His research interests include the fields of measurement, control, and microelectromechanical systems.

Dr. Zhou is the Vice President of China Instrument Society.